ARCHIVES
of
FOUNDRY ENGINEERING

ISSN (2299-2944)

10.24425/afe.2024.151288

Published quarterly as the organ of the Foundry Commission of the Polish Academy of Sciences

Comparison of the Mechanical Properties of Ductile Cast Iron Intended for Gas Gate Valves with Nickel Cast Iron with an Austenitic Matrix

A. Rączka [a] *, A. Szczęsny [b], D. Kopyciński [b]
[a] Fabryka Armatur JAFAR S.A. Kadyiego 12 Street
38-200 Jasło, Poland
[b] AGH University of Science and Technology, Faculty of Foundry Engineering,
Reymonta 23, 30-065 Kraków, Poland
* Corresponding author. e-mail address: arkadiusz.raczka23@gmail.com

Received 21.03.2024; accepted in revised form 13.06.2024; available online 22.07.2024

Abstract

The study presents a comparison of the results of structural tests, impact strength and strength properties of cast iron EN-GJS-400-15, which is produced in industrial conditions and the ductile cast iron, with addition of nickel, in austenitic matrix. Due to the ongoing energy transformation and attempts to inject hydrogen into existing gas grids, gas fittings manufacturers are looking for materials that will be more resistant to the destructive effects of hydrogen than the currently used ductile cast iron. The aim of the work was to obtain cast iron with the addition of nickel (about 20%) with similar strength parameters, better impact strength, both at room temperature and at lower temperatures, as well as a stable austenitic matrix in ductile cast iron. All assumptions were achieved. In the future, research should be undertaken to develop an economically optimal chemical composition, without a significant loss of strength properties, and the resistance of gate valves made of austenitic cast iron to the destructive effects of hydrogen should be examined. The work is preliminary research.

Keywords: Nodular cast iron, Austenitic matrix, Nickel cast iron, Impact strength

1. Introduction

In the pursuit of a sustainable energy future, hydrogen has become a key factor in the transition away from conventional fossil fuels. In 2020, the European Commission adopted a hydrogen strategy that aims to develop hydrogen production and its use. One of the key aspects of realizing hydrogen's full potential is its efficient transmission, and existing gas grids are an increasingly promising way to achieve this goal. The addition of hydrogen to natural gas can effectively reduce the combustion of natural gas and, therefore, carbon dioxide emissions. [1, 2]. According to research by the Oil and Gas Institute, it can be concluded that the maximum amount of hydrogen that can be safely injected into the gas grids is from 8% to 36%. It depends, among other things, on the range of pressures used, requirements regarding gas energy parameters, safety and effective combustion in final devices. [3]

Gas grids are complex infrastructure designed to transport natural gas from production sources to end users. One of the

elements of the gas grids and connection infrastructure is barrier and relief fittings. These elements are installed on low, medium and high pressure gas pipelines. They must be characterized by high resistance to maximum pressure and stresses that may occur in the gas grid. Gate valve bodies used and installed in gas pipelines should meet the requirements specified in Polish Standards and are often made of ductile cast iron, but also of steel or cast steel. [4, 5, 6]

Ductile cast iron is a durable material, but it is not resistant to hydrogen embrittlement [7], which may prove dangerous when a mixture of hydrogen and natural gas is used in gas grid. Hydrogen, being the smallest atom, is easily absorbed by materials, including cast iron. The test results [8] indicate that hydrogen in nodular cast iron is located at the graphite-ferrite interface, causing brittle fracture. The critical value of the graphite size in the microstructure is 13 µm. Exceeding this value increases the hydrogen absorption capability of ferritic ductile cast iron [9]. Hydrogen embrittlement is a phenomenon that can occur in various forms: Hydrogen blistering, Hydrogen Induced Cracking – HIC, Hydrogen Environment Assisted Cracking – HEAC, Stress-Oriented Hydrogen Induced Cracking – SOHIC, Sulphide Stress Cracking – SSC, Internal Hydrogen Assisted Cracking – IHAC. [10, 11]

Hydrogen resistant materials are metals, that resist the effects of hydrogen embrittlement or can operate stably in a hydrogen environment for extended periods of time. Alloys crystallizing in a face-centred cubic structure are characterized by greater resistance to hydrogen embrittlement compared to materials with a body-centred cubic structure. Therefore, most hydrogen resistant alloys are alloys with an austenitic matrix, such as austenitic steels or alloys based on iron and nickel. [12, 13]

High-nickel cast iron is characterized by good resistance to chemical and gas corrosion. It is achieved by the presence of nodular form of graphite but also by reducing the content of non-metallic inclusions during spheroidization. This reduces the tendency to create micro-cells responsible for the destruction of castings. [14]

A problem that may arise when producing nickel cast iron is the presence of unwanted martensite in the microstructure. [15, 16]

2. Research methodology

2.1. Technology of making ductile cast iron

One of the most frequently produced type of cast iron intended for valve elements for gas grids is EN-GJS-400-15 cast iron in accordance with the PN-EN 1563:2018-10 standard. It was smelted in medium-frequency electric induction furnace with a crucible capacity of 2 tons. Spheroidization was carried out at a station equipped with device for feeding a cored wire.

Table 1 shows the amount of individual charge materials used to melt the tested cast iron.

After melting the charge, the metal was overheated for 15 minutes at a temperature of about 1490ºC. After tapping into the ladle, the metal was subjected to spheroidization using a ⌀13 cored wire. Then, a test ingot of the „YII" type was poured in accordance with the PN-EN 1563 standard. During pouring, the in-stream method was used. A disc for chemical composition analysis also was poured. Analysis was carried out in the foundry's laboratory using a Spectro Analytical spectrometer, model SPECTROMAXx LMF04.

Table 1.
Content of charge materials.

Charge material	Quantity, kg
Special pig iron	930
Low-manganese unalloyed steel scrap	90
Scrap of ductile iron	1140
FeSi 75	21

The ingot was used to make samples for strength and impact tests in various temperature ranges, as well as a sample for hardness testing and metallographic. Tensile strength measurements were made on a ZIM machine (Soviet production), metallographic photos were taken on a Reichert microscope, model Me F2.

When discussing the results below, this cast iron will be referred to as Z1.

2.2. Using MAGMASOFT® to perform simulations

Due to the consideration of nickel cast iron as a material that could be used for the production of gate valves intended for gas grids with the addition of hydrogen, a pouring and solidification simulation was performed in the MAGMASOFT® 6.0 program, with particular emphasis on the occurrence of porosity that could cause material leakage and hydrogen penetration.

In order to carry out the simulation, the casting technology of the body valve, intended for gas gate valves, marked 2312 DN100, was used. Figure 1 shows the view of pouring system together with the arrangement of the bodies in the pouring mold and the cores, consistent with the actual arrangement of the bodies in the mold during production.

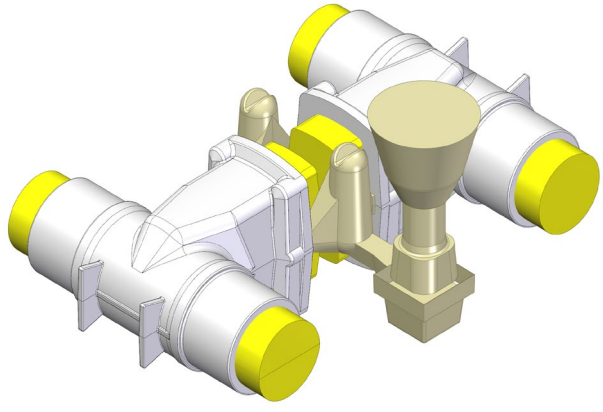

Fig. 1. Arrangement of castings and pouring system for simulation

2.3. Test melting of nickel cast iron

During the smelting of cast iron with the addition of nickel, the amount of charge materials presented in the table 2 was used.

Smelting was carried out in an induction furnace with a crucible capacity of 15kg. After melting the charge, the metal was heated to 1490°C and held for 10 minutes so that the process was as close as possible to the EN-GJS-400-15 cast iron produced at an earlier stage in industrial conditions. After heating the metal the crucible was removed from the furnace and transported to the spheroidization station using the bell method. After introducing the spheroidizer and modifier, the crucible returned to the furnace to collect slag. Then, samples were poured, i.e. a "YII" ingot, a disc for chemical composition analysis, a small Meehanite wedge and a small roller (the so-called finger test).

Table 2.
Amount of charge for melting cast iron with the addition of nickel

Charge material	Quantity, g
Special pig iron	1730
Low-manganese unalloyed steel scrap	3000
Scrap of ductile iron	5000
FeSi 75	20
Nickel cathode	2715
Carburizer	77
Spheroidizing agent	200
Modifier	36

A sample was taken from the ingot to test the strength properties, a sample to test the impact strength, a sample to test the hardness and make metallographic.

Strength, impact, hardness and metallurgical tests were performed on the same devices as cast iron marked as Z1, in the foundry laboratory. The analysis of the chemical composition, using the spectrometric method, was performed at the Optical Emission Spectrometer SPECTROMAXx.

When discussing the results, this type of tested cast iron was described as Z2.

3. Analysis of obtained results

3.1. Chemical composition and microstructure

As a result of melting the tested ductile cast iron Z1 and ductile cast iron with the addition of nickel Z2, the chemical composition given in table 3 was obtained.

Samples were taken from the cast ingots and metallographic were made. Figures 2 and 3 show the microstructure of Z1 cast iron. According to the PN-EN ISO 945-1:2019-09 standard, the shape of the graphite takes the form of nodule VI. After etching with a 3% Nital, a ferritic matrix can be observed.

Table 3.
Chemical composition of the tested cast iron.

Type of cast iron	Ni %	C %	Si %	Mg %	Mn %	S %	P %
Z1	0.024	3.63	2.48	0.048	0.12	0.012	0.039
Z2	21.76	2.17	1.83	0.034	0.1	0.0097	0.031

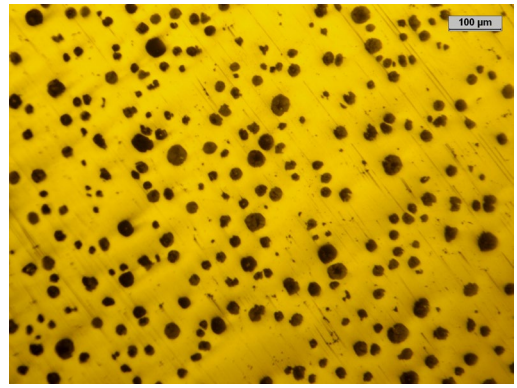

Fig. 2 Microstructure of cast iron Z1 in as-polished condition (x100)

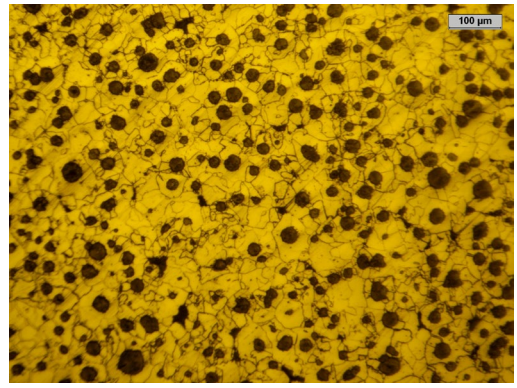

Fig. 3 Ferrite matrix of cast iron Z1(x100), etched 3% Nital

Figure 4 shows the microstructure of Z2 cast iron. In accordance with the PN-EN ISO 945-1:2019-09 standard, in this case precipitation of nodule graphite VI can also be observed. In some places it is degenerate and its shape resembles chunky graphite, which may be related to the content of 0,7% of rare earth metals in the spheroidizing agent, as well as to the addition of Al contained in the modifier. However, over 80% of the graphite precipitates have the correct spherical form. The size of graphite precipitates is smaller compared to Z1.

Figure 5 shows the austenitic matrix of Z2 cast iron with a content of approximately 15% bainite. The presence of austenite in the structure of cast iron is possible due to the appropriate nickel content, which shifts the range of austenite durability, even below room temperature. Figure 6 shows the same thing at a higher magnification (x500) and It was performed on a Leica MEF4M optical microscope using the Leica Q Win program (version 6).

Table 4.
Analysis of the chemical composition in micro-areas marked as in the figure 8

Elt.	Point 1		Point 2		Point 3		Point 4		Point 5		Point 6		Point 7		Point 8	
	Conc wt.%	Error 2-sig	Conc wt.%	Error 2-sig	Conc wt.%	Error 2-sig	Conc wt.%	Error 2-sig	Conc wt.%	Error 2-sig	Conc wt.%	Error 2-sig	Conc wt.%	Error 2-sig	Conc wt.%	Error 2-sig
Si	2.205	0.295	1.913	0.282	2.217	0.301	2.040	0.291	2.090	0.297	1.932	0.287	1.346	0.243	1.898	0.281
P	0.000	0.000	0.051	0.042	0.075	0.050	0.025	0.029	0.191	0.081	0.087	0.055	0.110	0.062	0.011	0.020
S	0.120	0.055	0.036	0.031	0.115	0.054	0.147	0.062	0.137	0.060	0.027	0.027	0.101	0.052	0.028	0.027
Mn	0.071	0.029	0.046	0.024	0.171	0.046	0.069	0.030	0.063	0.029	0.023	0.017	0.060	0.028	0.036	0.021
Fe	76.163	1.453	75.055	1.474	81.519	1.547	78.705	1.519	78.033	1.527	77.939	1.529	76.209	1.525	77.148	1.498
Ni	21.441	0.974	22.898	1.029	15.903	0.864	19.014	0.944	19.486	0.964	19.990	0.979	22.174	1.040	20.878	0.985

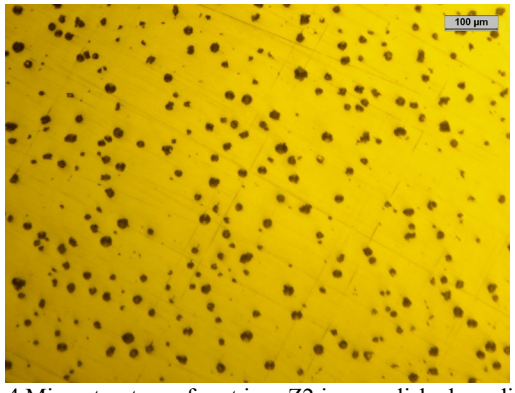

Fig. 4 Microstructure of cast iron Z2 in as-polished condition (x100)

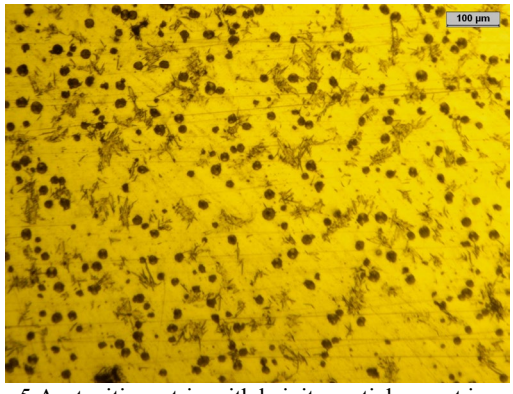

Fig. 5 Austenitic matrix with bainite particles, cast iron Z2 (x100), etched 3% Nital

Figure 7 shows a photo of the microstructure of austenitic cast iron with the addition of nickel, which was taken on a SEM JEOL 500LV microscope with an X-ray microanalysis (EDS). Observation of the precipitates at x1000 magnification reveals their heterogeneity. There are at least several precipitates, light and dark phases, as well as graphite and characteristic sharp bainite precipitates. All these separations are also clearly visible in Figure 6.

It was decided to analyse the chemical composition of individual micro-areas. 8 points were determined, which are shown in figure 8, and the results obtained are presented in Table 4. However, this method does not allow to clearly determine the type of phases observed. The results indicate similar content of elements at individual points. The content of silicon clearly differs from the others in point 7. This is the brightest place of all and is characterized by a lower content of this element. The content of iron and nickel is also different from the others in point 3. Iron reaches its highest measured value, while nickel has the lowest.

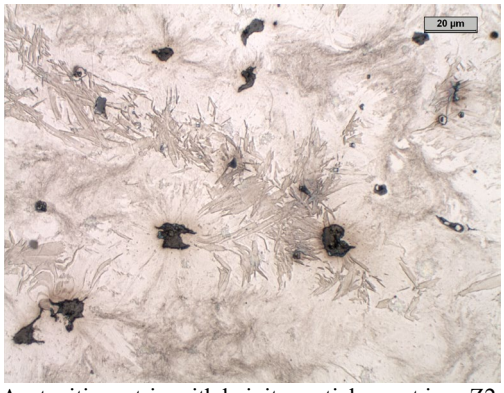

Fig. 6 Austenitic matrix with bainite particles cast iron Z2 (x500) etched 6% Nital

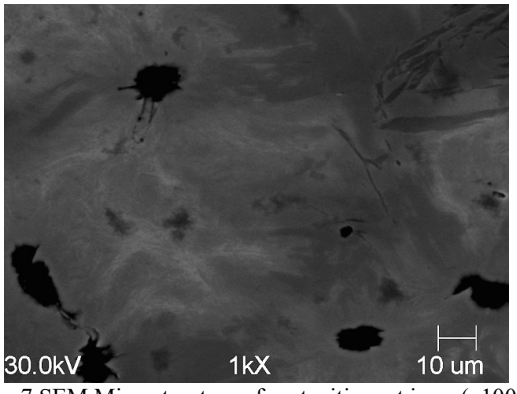

Fig. 7 SEM Microstructure of austenitic cast iron. (x1000)

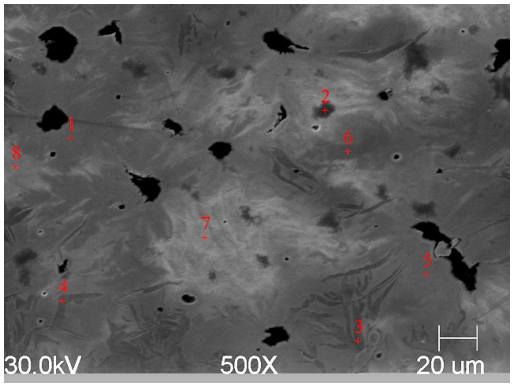

Fig. 8 Microstructure of cast iron Z2 with marked areas

Based on figures 2 and 4, measurements of graphite precipitation were made. As can be seen, the size of the precipitates and their number are different, even though the samples for metallographic examination were taken from the same places of poured ingots. The average radius of graphite nodules for cast iron Z1 from figure 2 is 16,54 µm, while for cast iron Z2 it is 10,87 µm. Table 5 presents the results showing the number of graphite precipitations per mm^2 and graphite surface. The share of graphite in the microstructure of cast iron Z1 is higher than that of cast iron Z2 and amounts to 16% and 8%, respectively. On the other hand, the number of graphite precipitations of Z2 cast iron is higher and amounts to 546,46 compared to 378,17 for Z1 cast iron, which confirms the visible difference in the compared figures.

Table 5.
Comparison of the number of graphite precipitations.

Type of cast iron	Graphite surface %	Number of graphite precipitations per mm^2
Z1	16%	378,17
Z2	8%	564,46

3.2. Mechanical properties

Impact strength testes were carried out at room temperature (23±5)ºC, (0±2)ºC and (-20±2)ºC. For each temperature, measurements were made on 3 samples, then the average was drawn, based on which, figure 9 was made. Before carrying out the test, each sample was held at the appropriate temperature for 5 minutes, then placed on a Charpy Hammer and tested. Tables 6 and 7 present the results of each separate sample and the average of 3 measurements at a given temperature.

After comparing the results, it can be seen that as the temperature decreases, the impact strength of Z1 cast iron decreases from 21,87J at room temperature, through 15,83J at 0ºC, to 14,37J at -20ºC.

The situation is different in the case of Z2 cast iron. The impact strength begins to increase as the temperature decreases. This increase is imperceptible, from 54,6J at room temperature to 54,9J at 0ºC. A greater increase can be observed at -20ºC, the result being 57,8J.

Comparing both tested types of cast iron, it can be concluded that cast iron with an austenitic matrix has significantly higher impact strength both at room and low temperatures. The high impact strength of Z2 cast iron results from the presence of austenite in the microstructure, which is a plastic component of alloys. The high parameter obtained at a reduced temperature also confirms that austenite is still present.

Table 6.
Impact strength results for cast iron Z1

Sample no	Impact strength KV, J		
	Temperature 23ºC	Temperature 0ºC	Temperature -20ºC
1	24,5	13,7	15,7
2	21,5	19,6	13,7
3	19,6	14,2	13,7
Average of 3 measurements	21,87	15,83	14,37

After preparing strength samples taken from test ingots, the strength properties R_m, $R_{0,2}$, elongation A and hardness were tested. Table 8 compares the results of individual properties of both tested alloys.

Table 7.
Impact strength results for cast iron Z2

Sample no	Impact strength KV, J		
	Temperature 23ºC	Temperature 0ºC	Temperature -20ºC
1	55,9	59,8	60,8
2	52	55,9	56,9
3	55,9	49	55,9
Average of 3 measurements	54,6	54,9	57,8

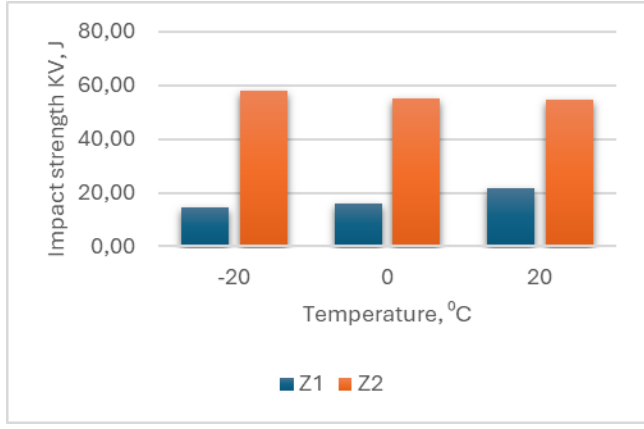

Fig. 9 Influence of temperature on impact strength

Table 8.
Comparison of strength properties

Material	R_m, MPa	$R_{p0,2}$, Mpa	A_5, %	Hardness, HB
Z1	467,7	361,6	22	156
Z2	517,5	214,6	13	145

The analysis of the results presented in table 8 shows that, as expected, EN-GJS-400-15 cast iron was obtained from the sample marked Z1. Due to the ferritic structure, a hardness of 156 HB and an elongation of as much as 22% were achieved. Sample Z2 with the addition of nickel has a similar hardness of 146 HB and a much lower elongation, namely 13%, as well as the conventional yield strength. However, the obtained tensile strength is higher and amounts to 517 MPa. The increased strength is related to the presence of smaller particles of nodule graphite in the microstructure. Based on the above strength results, it can be concluded that this cast iron is suitable for components intended for gas grids, although castings would have to be made and tested in accordance with the PN-EN 13774:2013-07 standard.

3.2. Results of simulations in MAGMASOFT®

First, a valve body was simulated with chemical composition consistent with the results obtained for Z1 alloy, The pouring temperature was assumed to be 1400ºC. Figure 10 shows the simulation results, more specifically the porosity occurring inside the casting. The x-ray display parameter has been set above 10%.

The porosity was located mainly in the thicker parts of the casting, away from the gating system. Porosity is also visible in the place where the liquid metal enters the mold cavity, but it is much smaller than the rest of the defects.

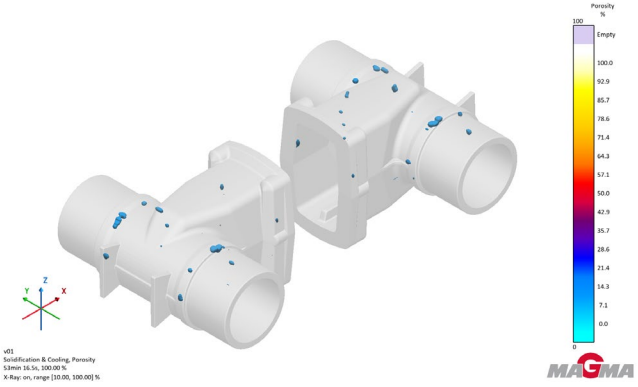

Fig. 10 Porosity cast iron Z1, x-ray 10%

Then, an adequate simulation process was performed for the same detail with the same pouring parameters as for the Z1 alloy. The chemical composition was changed and the composition consistent with the obtained for the Z2 alloy was introduced. The x-ray parameter was also set above 10% in this case.

The simulation results are shown in figure 11. It shows that the area of porosity and its size have significantly decreased. They are still located in the thicker part of the casting, but they are much smaller compared to the Z1 alloy.

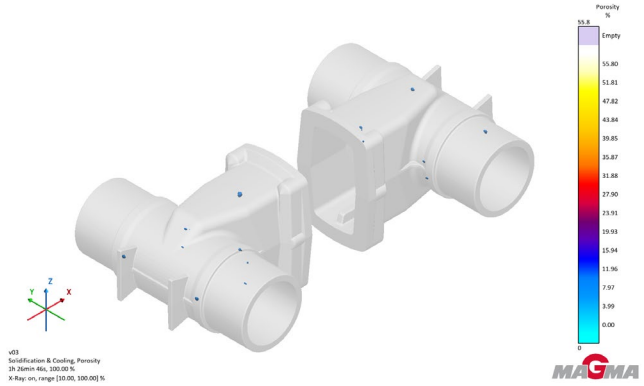

Fig. 11 Porosity cast iron Z2, x-ray 10%

4. Conclusions

The conducted research allowed us to draw the following conclusions.

1. Ductile cast iron with the addition of nickel tested in this publication achieves similar strength parameters to standard EN-GJS-400-15 cast iron. Moreover, it obtains a higher tensile strength Rm, exceeding the threshold of 500 MPa, with a 9% decrease in the elongation valuer. The presence of austenite in the structure resulted in an increase in tensile strength, while the decrease in elongation is due to the presence of bainite in the microstructure, therefore efforts should be made to eliminate this unfavourable component. Industrial test should be carried out, consisting in the production of Z2 cast iron gate valve elements intended for installation in gas grids and subjected to a pressure test to check tightness and durability.
2. The obtained nickel ductile iron has increased impact strength in each tested temperature range compared to standard cast iron type EN-GJS-400-15. The austenite in the microstructure is responsible for the high impact strength. As the temperature decreases, the impact strength of the alloy begins to slowly increase, which is also a good prognosis for the production of components made of this type of alloy, especially those intended for assembly in an environment with a reduced ambient temperature.
3. Nickel increases the tendency to form an austenitic matrix and promotes graphitization by extending the eutectic temperature range. However, it should strive to keep the content of this element in cast iron as low as possible due to the tendency to develop bainite. For this purpose, it would be necessary to select the appropriate Si content and additionally bring in Mn into the alloy to reduce the tendency to make carbides. Moreover, reducing the nickel content will also result in competitive market prices in the production of cast iron with a stable austenitic matrix.
4. Simulation performed using MAGMASOFT® software confirms the decreased tendency to porosity with the addition of nickel. This is of great importance when considering nickel cast iron with an austenitic matrix for the production of gate valves that require tightness.

5. If the foundry decided to implement nickel cast iron production, the tightness of valves made of austenitic cast iron and standard ductile cast iron should be tested for tightness with particular emphasis on the tightness of hydrogen permeability. The service life and safe operation of both gate valves with different hydrogen contents also need to be compared. Moreover, if the research were to continue, it would be possible to take EBSD images, as it was not necessary given the preliminary nature of the research that was performed here.

Acknowledgements

Melting and tests were made possible thanks to the Faculty of Foundry Engineering of AGH University of Science and Technology and Fabryka Armatur "JAFAR" S.A.

References

[1] Kanellopoulos, K., Busch, S., De Felice, M., Giaccaria, S. & Costescu, A. (2022). *Blending hydrogen from electrolysis into the European gas grid*. EUR 30951 EN, Publications Office of the European Union, Luxembourg, 2022, ISBN 978-92-76-46346-7, DOI:10.2760/908387, JRC 126763.

[2] ToGetAir. (2024). *Hydrogen Needs Strong Support*. Retrieved December, 18, 2023 from https://raport.togetair.eu/ogien/energia-przyszlosci/wodor-potrzebuje-mocnego-wsparcia. (in Polish).

[3] Jaworski, J., Kukulska-Zając, E. & Kułaga, P. (2019). Selected issue regarding the impact of addition of hydrogen to natural gas on the elements of the gas system. *Nafta-Gaz*. 10, 625-632. DOI: 10.18668/NG.2019.10.04. (in Polish).

[4] Bąkowski, K, (2007). *Gas grids and installations – guide*. Warszawa: WNT. (in Polish).

[5] EN 13774:2013 Valves for gas distribution system with maximum operating pressure less than or equal to 16 bar – Performance requirements.

[6] Regulation of the Minister of Economy of April 26, 2013 on the technical conditions to be met by gas grids and their location. (Dz.U z 2013 r., Nr 0, poz. 640). (in Polish).

[7] Information Publication 11/I, Safe use of hydrogen as fuel in commercial industrial applications, Polish Ship Register, Gdańsk 2021, p 36 (in Polish)

[8] Sahiluoma, P., Yagodzinskyy, Y., Forsström, A., Hänninen, H. & Bossuyt, S. (2021). Hydrogen embrittlement of nodular cast iron. *Materials and Corrosion*. 72(1-2), 245-254. DOI: 10.1002/maco.202011682.

[9] Yoshimoto, T., Matsuo, T. & Ikeda, T. (2019). The effect of graphite size on hydrogen absorption and tensile properties of ferritic ductile cast iron. *Procedia Structural Integrity.* 14, 18-25. https://doi.org/10.1016/j.prostr.2019.05.004.

[10] Elboujdaini E. (2011). *Hydrogen-Induced Cracking and Sulfide Stress Cracking.* Uhlig's Corrosion Handbook. R. Winston Revie (red.). Wiley, 183-194.

[11] Gangloff, R.P. (2012). *Gaseous hydrogen embrittlement of materials in energy technologies.* Woodhead Publishing.

[12] Jiaxing Liu, Mingjiu Zhao, Lijian Rong (2023). Overview of hydrogen-resistant alloys for high-pressure hydrogen environment: on the hydrogen energy structural materials. *Clean Energy.* 7(1), 99-115. https://doi.org/10.1093/ce/zkad009.

[13] Dwivedi, S.K. & Vishwakarma. M. (2018). Hydrogen embrittlement in different materials: A review. *International Journal of Hydrogen Energy.* 43(46), 21603-21616. https://doi.org/10.1016/j.ijhydene.2018.09.201.

[14] Dziadur, W., Lisak, J., & Tabor A. (2004). Corrosion testing of high-nickel ductile cast iron. *Journal of Applied Materials Engineering.* 6, 28-32. (in Polish).

[15] Guzik, E., Kopyciński, D. (2004). Structure and impact strength of austenitic ductile iron. *Archives of Foundry*. 4(12), 115-120. ISSN 1642-5308. (in Polish).

[16] Tabor, A., Putyra, P., Zarębski, P. & Maguda, T. (2009). Austenitic ductile iron for low temperature applications. *Archives of Foundry Engineering.* 9(1), 163-168. ISSN (1897-3310).